

# A positional Toll receptor code directs convergent extension in *Drosophila*

Adam C. Paré<sup>1</sup>, Athea Vichas<sup>1</sup>, Christopher T. Fincher<sup>1</sup>, Zachary Mirman<sup>1</sup>, Dene L. Farrell<sup>1</sup>, Avantika Mainieri<sup>1</sup> & Jennifer A. Zallen<sup>1</sup>

**Elongation of the head-to-tail body axis by convergent extension is a conserved developmental process throughout metazoans. In *Drosophila*, patterns of transcription factor expression provide spatial cues that induce systematically oriented cell movements and promote tissue elongation. However, the mechanisms by which patterned transcriptional inputs control cell polarity and behaviour have long been elusive. We demonstrate that three Toll family receptors, Toll-2, Toll-6 and Toll-8, are expressed in overlapping transverse stripes along the anterior-posterior axis and act in combination to direct planar polarity and polarized cell rearrangements during convergent extension. Simultaneous disruption of all three receptors strongly reduces actomyosin-driven junctional remodelling and axis elongation, and an ectopic stripe of Toll receptor expression is sufficient to induce planar polarized actomyosin contractility. These results demonstrate that tissue-level patterns of Toll receptor expression provide spatial signals that link positional information from the anterior-posterior patterning system to the essential cell behaviours that drive convergent extension.**

A central question in developmental biology is how the diverse structures of multicellular tissues are generated on a cellular and molecular level. Convergent extension, in which a tissue narrows along one axis and lengthens in a perpendicular direction, is a conserved tissue remodelling process that elongates the head-to-tail body axis of many animals. Cell intercalation provides the driving force for convergent extension in frogs, fish, flies, chicks and mice<sup>1–5</sup>. This process is characterized by a striking directionality in which hundreds of cells align their movements along a common axis. In epithelial tissues, cell intercalation is mediated by spatially regulated actomyosin contractility, which induces locally oriented cell rearrangements that produce concerted elongation at the tissue scale<sup>6–10</sup>. This mechanism was first discovered in *Drosophila*<sup>6–10</sup>, and has since been shown to promote convergent extension in the vertebrate neural plate, primitive streak, kidney and notochord<sup>11–16</sup>. In *Drosophila* and *Xenopus*, the spatial cues that align cell movements with the tissue axes are not cell-intrinsic or long-range secreted signals. Instead, contact-dependent signals provide the critical spatial inputs that orient cell intercalation<sup>6,17,18</sup>. In the *Drosophila* embryo, these inputs are mediated by the pair-rule transcription factors Eve and Runt, components of the embryonic anterior-posterior (AP) patterning system that are expressed in transverse stripes along the AP axis<sup>19</sup>. When these striped patterns are disrupted, either in *eve* or *runt* mutants or in embryos overexpressing Eve or Runt at high levels, intercalary behaviours are reduced and misoriented<sup>8,17,20</sup> and the actomyosin contractile machinery becomes mislocalized within cells<sup>6,8,21</sup>. Ectopic Eve or Runt expression perpendicular to their normal stripes is sufficient to reorient planar polarity in intercalating cells<sup>6</sup>, demonstrating that spatial patterns of Eve and Runt activity provide instructive polarity cues. However, the connection between transcriptional information provided by striped patterns of Eve and Runt activity and the effector molecules that generate polarized cell behaviour during convergent extension has long been elusive<sup>2,22</sup>.

## A positional code of Toll receptor stripes

To identify the targets of Eve and Runt that direct cell behaviour during convergent extension, we performed RNA sequencing on *Drosophila* embryos co-injected with *eve* and *runt* double-stranded RNAs (dsRNAs). Compared with water-injected controls, 42 genes were differentially

expressed ( $P < 0.01$ , Extended Data Fig. 1a–c and Supplementary Table 1). As Eve and Runt can function as transcriptional repressors, we focused on the 24 genes that were significantly upregulated by *eve/runt* RNA interference (RNAi). This group included *Toll-8* (also known as *Tollo*), which encodes a single-pass transmembrane protein containing 27 extracellular leucine-rich repeats (LRRs) and a conserved cytoplasmic Toll/interleukin-1 receptor (TIR) domain. The related gene *Toll-2* (also known as *18-wheeler*) was also upregulated by *eve/runt* RNAi. Toll-2 and Toll-8 belong to the Toll receptor family that regulates innate immunity in arthropods and vertebrates<sup>23–27</sup>. The founding member of this family, Toll, is essential for dorsal-ventral patterning in *Drosophila*<sup>28</sup>, and the paralogues *Toll-2*, *Toll-6*, *Toll-7* and *Toll-8* are expressed in stripes in patterns reminiscent of the pair-rule genes<sup>29–31</sup>. As members of this family can influence cell adhesion and epithelial morphology<sup>31–35</sup>, we focused on Toll receptors as candidate effectors of Eve and Runt that could regulate polarized cell behaviour during convergent extension.

To determine whether the striped expression of Toll family receptors requires Eve and Runt activity, we analysed their expression by fluorescence *in situ* hybridization<sup>36</sup>. In wild-type embryos, *Toll-2* is expressed in 13 stripes in the germband, of which the odd-numbered stripes coincide with Runt (Fig. 1a, d and Extended Data Fig. 2a, d)<sup>29–31</sup>. *Toll-6* and *Toll-8* are each expressed in 6 partially overlapping stripes, with *Toll-6* expressed anterior to the stripes of high *Toll-2* expression and *Toll-8* expressed between them (Fig. 1b, c, e, f, m, n and Extended Data Fig. 2b, c, e, f). *Toll-7* was detected at low levels during axis elongation (Extended Data Fig. 1d and Supplementary Table 1). The 13 *Toll-2* stripes collapsed into 6 broad stripes in *eve* and *runt* mutants (Fig. 1g, j). *Toll-6* levels were reduced and *Toll-8* was nearly absent in *eve* mutants (Fig. 1h, i), whereas *Toll-6* and *Toll-8* were upregulated and more uniformly expressed in *runt* mutants (Fig. 1k, l). The Toll-8 protein fused to YFP and expressed from its endogenous regulatory sequences localized to the plasma membrane, with cells in the middle of each stripe showing stronger signal with no obvious overall planar polarity (Fig. 1o). Therefore, neighbouring cells along the AP axis express different combinations of *Toll-2*, *Toll-6* and *Toll-8* in an Eve- and Runt-dependent pattern (Fig. 1p).

<sup>1</sup>Howard Hughes Medical Institute and Developmental Biology Program, Sloan Kettering Institute, New York, New York 10065, USA.

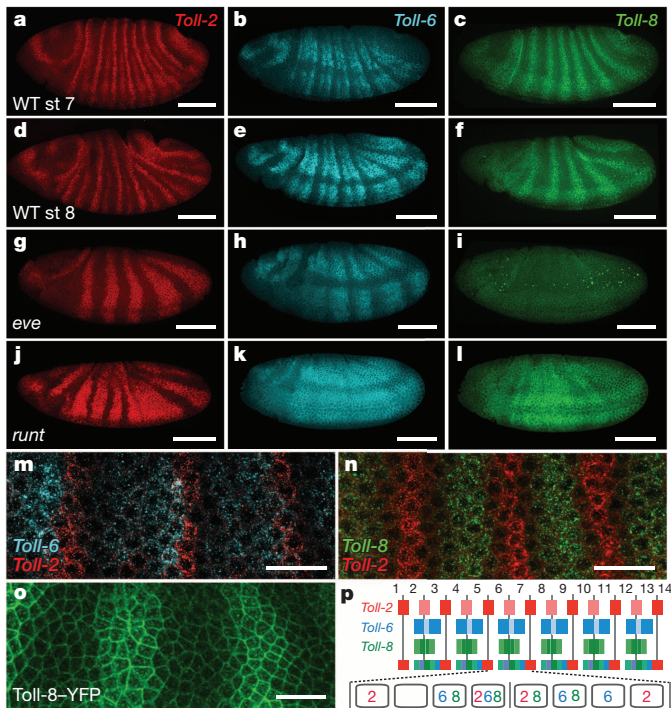


**Figure 1 | Cells express different combinations of Toll-2, Toll-6 and Toll-8 along the anterior-posterior axis.** **a–n**, Toll-2 (red), Toll-6 (cyan) and Toll-8 (green) mRNA expression in wild-type (WT) embryos during early (stage 7, **a–c**, **m**, **n**) and mid-elongation (stage 8, **d–f**). **a–f**, WT embryos; **g–i**, *eve* mutant; **j–l**, *runt* mutant. **m**, **n**, Toll-6 (cyan) is expressed anterior to the strong Toll-2 stripes (red) and Toll-8 (green) is expressed between them. **o**, Toll-8-YFP protein in a stage 7 Toll-8 mutant. **p**, Schematic of Toll-2, Toll-6 and Toll-8 expression. Numbers, parasegments; vertical lines, parasegmental boundaries. Anterior left, ventral down. Scale bars, 100  $\mu$ m (**a–l**), 20  $\mu$ m (**m–o**).

## Toll receptors direct cell intercalation

We next investigated whether Toll-2, Toll-6 and Toll-8 are required for convergent extension, as predicted for the targets of Eve and Runt that control cell behaviour. The wild-type germband epithelium doubles in length along the AP axis within the first 30 min of elongation ( $2.00 \pm 0.07$ -fold increase in length) (Fig. 2a–c). Axis elongation occurred normally in Toll-8 single mutants (Fig. 2c and Extended Data Fig. 3a, b, f). Therefore, we postulated that multiple Toll receptors act together to regulate cell behaviour during elongation. To disrupt multiple Toll receptors simultaneously, we injected dsRNAs that specifically target Toll-2 and Toll-6 into Toll-8 null mutant embryos (Extended Data Fig. 1e, f). Embryos defective for any one receptor elongated to a wild-type extent (Fig. 2b, c and Extended Data Fig. 3a, b, f). By contrast, axis elongation was reduced by nearly 20% in embryos defective for Toll-2 and Toll-6 ( $1.83 \pm 0.03$ -fold,  $P < 0.02$ ) and nearly 40% in embryos defective for Toll-2, Toll-6 and Toll-8 ( $1.61 \pm 0.04$ -fold,  $P < 0.001$ ) (Supplementary Video 1), similar to *eve* and *runt* mutants ( $1.68 \pm 0.05$ -fold in *eve* and  $1.64 \pm 0.02$ -fold in *runt*,  $P < 0.01$ ) (Fig. 2c and Extended Data Fig. 3d, f). In addition, we used TAL effector nucleases (TALENs)<sup>37</sup> to generate embryos that completely lack Toll-2, Toll-6 and Toll-8, and found that Toll-2,6,8 triple mutants display a significant reduction in axis elongation (Fig. 2b, c, Extended Data Figs 3e, f and 4 and Supplementary Video 2). These results demonstrate that Toll-2, Toll-6 and Toll-8 act in combination to regulate axis elongation.

Cell intercalation is the primary mechanism driving axis elongation in *Drosophila*<sup>7,8,17</sup>. To determine whether Toll receptors are required for cell intercalation, we used automated methods to track cell behaviour in time-lapse movies<sup>21,38</sup>. In embryos defective for any one Toll family receptor, the frequency of cell intercalation was similar to wild type (Fig. 2f and Extended Data Fig. 3a, b, g–i). By contrast, cell intercalation

was reduced by 17% in embryos defective for Toll-2 and Toll-6 ( $P < 0.03$ ), 19% in embryos defective for Toll-6 and Toll-8 ( $P < 0.02$ ), and more than 30% in Toll-2,6,8 triple mutants ( $P < 0.001$ ), accompanied by slower edge contraction (Fig. 2e, f and Extended Data Fig. 3c–e, g–j). Toll-2,6,8 triple mutants were similar to *runt* mutants, although not quite as severe as *eve* mutants (Fig. 2e, f; Extended Data Fig. 3e, g–i). These results demonstrate that Toll-2, Toll-6 and Toll-8 promote cell intercalation during axis elongation.

For cell rearrangements to produce tissue elongation, intercalation must occur directionally through the contraction of interfaces between anterior and posterior neighbours (AP edges) and the formation of interfaces between dorsal and ventral neighbours (DV edges) (Fig. 2d)<sup>7,8</sup>. Contracting edges were correctly oriented in all Toll receptor-defective embryos (Extended Data Fig. 3k). By contrast, in more than one-third of cell rearrangements in Toll-2,6,8 mutants, new edges failed to form, were unstable, or formed in the wrong direction ( $36 \pm 4\%$  of edges in Toll-2,6,8 vs  $9.5 \pm 0.3\%$  in wild type,  $P < 0.0001$ ), similar to the defects in *eve* and *runt* mutants ( $34 \pm 4\%$  in *eve* and  $37 \pm 1\%$  in *runt*,  $P \leq 0.01$ ) (Fig. 2g). Embryos defective for Toll-2 alone had intermediate defects, indicating that the other Toll receptors cannot fully substitute for Toll-2 in orienting edge formation. These results indicate that Toll receptors are required for rapid edge contraction and directional edge formation, suggesting that a common mechanism underlies both steps of cell rearrangement. Physical forces generated by the intercalation of subsets of cells can reinforce myosin polarity<sup>10</sup> and trigger passive cell stretching in neighbouring cells<sup>20</sup>, perhaps allowing for substantial elongation in embryos that express a partial complement of Toll receptors.

## Toll receptors and planar polarity

Cell intercalation in *Drosophila* is driven by the planar polarized activity of myosin II, which promotes the contraction of AP edges<sup>6–10</sup>, and Par-3, which excludes myosin and stabilizes adhesion at DV edges<sup>6,21</sup>. To determine whether Toll receptors are required for myosin II and Par-3 localization, we used automated methods to analyse planar polarity at single-cell resolution<sup>39</sup>. In wild-type embryos, myosin II was enriched  $1.30 \pm 0.02$ -fold at AP edges and Par-3 was enriched  $1.71 \pm 0.03$ -fold at DV edges (Fig. 3a, e, f). By contrast, Toll-2,6,8 mutants had a 47% reduction in myosin II planar polarity ( $1.16 \pm 0.01$ ,  $P < 0.0001$ ) and a 48% reduction in Par-3 planar polarity ( $1.37 \pm 0.02$ ,  $P < 0.0001$ ) (Fig. 3b, e, f). Similar defects were observed in *runt* mutants, although planar polarity was more severely affected in *eve* mutants ( $1.21 \pm 0.01$  for Par-3 and  $1.09 \pm 0.02$  for myosin,  $P < 0.0001$ ) (Fig. 3c–f and Extended Data Fig. 5). Toll receptor expression is reduced in *eve* mutants, whereas *runt* mutants have increased expression (Fig. 1g–l), suggesting that distinct mechanisms may underlie the defects in these two backgrounds. Apical-basal polarity was unaffected in Toll receptor mutants (Extended Data Fig. 3l), and planar polarity was not further reduced in Toll-2,6,7,8 quadruple mutants (Extended Data Fig. 5g, h). These results demonstrate that Toll-2, Toll-6 and Toll-8 act together to regulate myosin II and Par-3 planar polarity.

Par-3 and myosin II planar polarity displayed regional differences in Toll-2 mutants. Planar polarity occurred normally in Toll-8-expressing cells, most of which also express Toll-6, but was significantly reduced in Toll-8-negative cells, the majority of which do not express any Toll receptors (Fig. 3e, g, i and Extended Data Fig. 6a). Similarly, in Toll-6,8 mutants, Toll-2-expressing cells had wild-type planar polarity, whereas cells that did not express any of these receptors had significant defects (Fig. 3h, j). Therefore, embryos expressing only one or two Toll receptors have localized planar polarity defects in the regions of missing receptor expression.

In *eve* mutants, which almost completely lack planar polarized myosin, residual myosin cables still form at the posterior boundaries of Toll-2 stripes (Fig. 4d and Extended Data Fig. 6b, c), suggesting that differences in Toll receptor activity may induce planar polarity. To test this, we expressed Toll-2 and Toll-8 in stripes in the late embryo using the *engrailed-Gal4* driver. The anterior boundary of each *engrailed* stripe



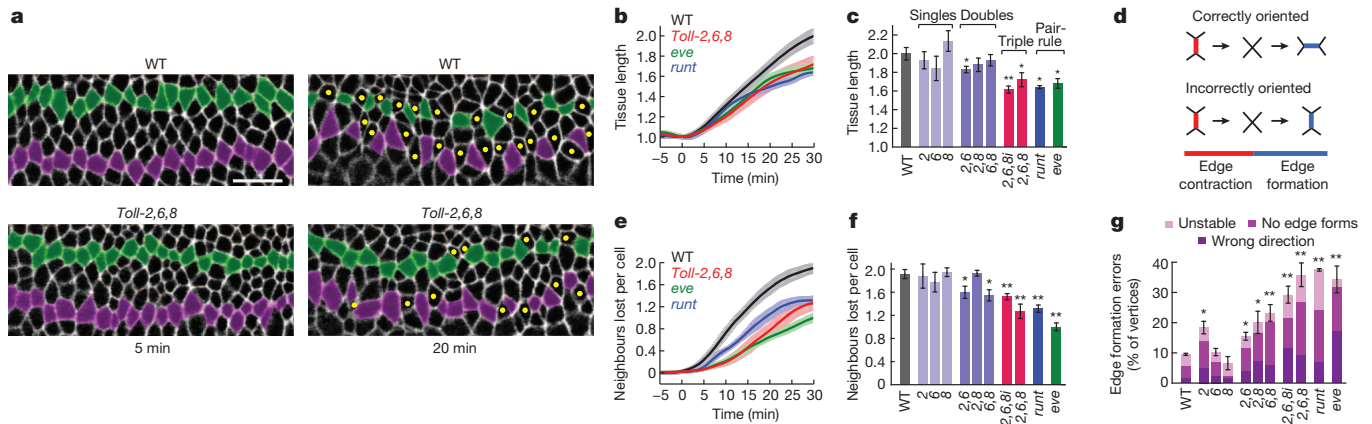


**Figure 2 | Toll-2, Toll-6 and Toll-8 regulate cell intercalation and axis elongation.** **a**, Stills from time-lapse movies of a wild-type (WT) embryo (top) and a *Toll-2* and *Toll-6* dsRNAs (*Toll-2,6,8*) (bottom). Resille-GFP (white). *t* = 0, onset of elongation. In wild type, nearly all initially adjacent cells become separated by intercalated cells (yellow dots). In *Toll-2,6,8* embryos, many cells fail to separate. Anterior left, ventral down. Scale bar, 20  $\mu$ m. **b, c**, Axis elongation (tissue AP length relative to *t* = 0) over time (**b**) and at 30 min (**c**). **d**, Edge contraction and formation. **e, f**, Cell rearrangements over time (**e**) and at 30 min (**f**). Single average values were obtained for each embryo; plots show the mean  $\pm$  s.e.m. across embryos.

is situated anterior to the denticle-forming cells, in a region where myosin II is not strongly planar polarized (Fig. 4a). Ectopic Toll-2 or Toll-8 led to a strong recruitment of myosin II to the anterior boundary of the *engrailed* domain (Fig. 4b, c, e and Supplementary Videos 3–5) and increased contractile activity at this boundary, as measured by laser ablation (Fig. 4f). These results demonstrate that local differences in Toll-2 or Toll-8 expression are sufficient to induce myosin planar polarity *in vivo*.

### Heterophilic Toll receptor interactions

*Drosophila* Toll receptors are known to bind to Spätzle/DNT neurotrophin-related growth factors<sup>23,28,40,41</sup>, but the ligands detected by Toll receptors during convergent extension are not known. In one model, heterophilic

**b–f**, *n* = 3–8 embryos per genotype, 164–365 cells per embryo (Supplementary Table 2). **g**, Edge formation errors. *n* = 3–9 embryos per genotype, 42–104 vertices per embryo. \**P* = 0.01–0.03, \*\**P* < 0.005 (unpaired *t*-test). WT (*Spider-GFP*); 2 (*Resille-GFP* + *Toll-2* dsRNA); 6 (*Resille-GFP* + *Toll-6* dsRNA); 8 (*Resille-GFP*; *Toll-8*<sup>59/145</sup>); 2,6 (*Resille-GFP* + *Toll-2/Toll-6* dsRNAs); 2,8 (*Resille-GFP*; *Toll-8*<sup>59/145</sup> + *Toll-2* dsRNA); 6,8 (*Toll-2*<sup>Δ76</sup>/*CyO*; *Toll-8*<sup>59</sup>, *Toll-6*<sup>5A</sup>, *Spider-GFP*); 2,6,8 (*Resille-GFP*; *Toll-8*<sup>59/145</sup> + *Toll-2/Toll-6* dsRNAs); 2,6,8 (*Toll-2*<sup>Δ76</sup>, *Toll-8*<sup>59</sup>, *Toll-6*<sup>5A</sup>, *Spider-GFP*); *runt* (*runt*<sup>L85</sup>; *Spider-GFP*); *eve* (*eve*<sup>R13</sup>; *Spider-GFP*).

interactions between receptors expressed on adjacent stripes of cells could induce actomyosin contractility at AP cell edges. Alternatively, homophilic interactions between receptors expressed in the same stripe could suppress actomyosin contractility and stabilize adhesion at DV edges. To investigate these possibilities, we tested for interactions between Toll receptors in *Drosophila* S2R+ cells<sup>42</sup>. Cells expressing Toll-2 displayed increased affinity for a soluble, pentamerized form of the Toll-8 extracellular domain (Fig. 5a, b). By contrast, cells expressing Toll-2 displayed decreased affinity for the Toll-2 extracellular domain (Fig. 5c, d). These results indicate that Toll-2 and Toll-8 can interact in a heterophilic manner in cultured cells.

To test whether Toll receptors can promote interactions between cells, we performed cell-mixing experiments. *Drosophila* S2R+ cells

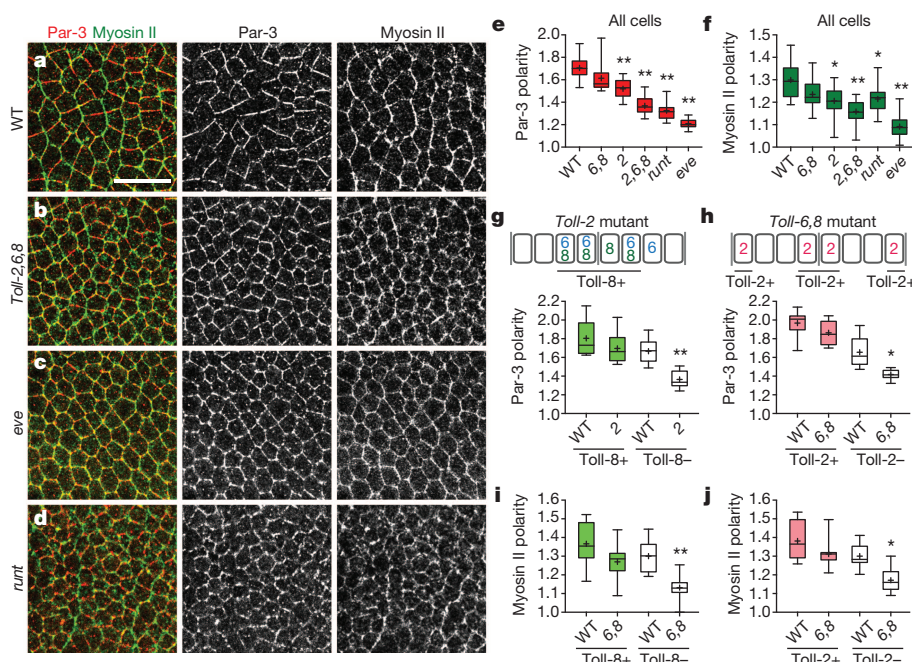


**Figure 3 | Toll receptors are required for myosin II and Par-3 planar polarity.** **a–d**, Stage 7 wild-type (**a**), *Toll-2,6,8* (**b**), *eve* (**c**) and *runt* (**d**) embryos. Par-3 (red, middle), myosin II (green, right). **e–j**, Par-3 and myosin II planar polarity in all cells (**e, f**) and subsets of cells (**g–j**). Horizontal line, median; +, mean; boxes, second and third quartiles; whiskers, 95% confidence interval. Single average values were obtained for each embryo; plots show the distribution of values across embryos. \**P* ≤ 0.005, \*\**P* < 0.0001 (unpaired *t*-test). *n* = 11–19 embryos per genotype; 2,445–4,698 cells per embryo (Supplementary Table 2). Anterior left, ventral down. Scale bar, 20  $\mu$ m.

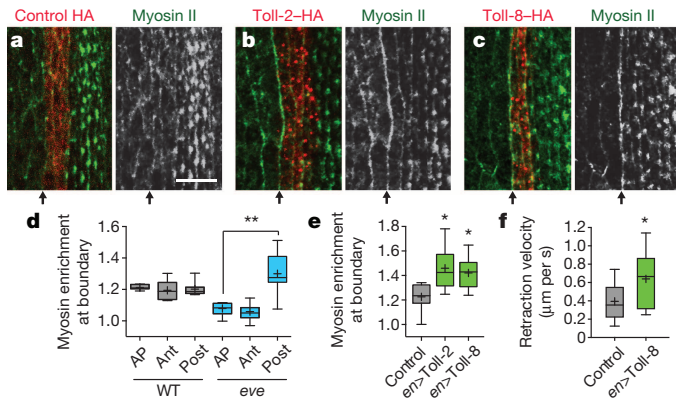


**Figure 4 | Myosin II localization and activity are enhanced at boundaries of Toll-2 and Toll-8 expression.** **a–c**, Stage 15 embryos expressing control  $\beta$ -catenin-HA (**a**), Toll-2-HA (**b**), or Toll-8-HA (**c**) expressed with *engrailed-Gal4*. Myosin II (green, white), HA (red). Arrows, anterior boundary of the *engrailed* domain. Ventral views. Scale bar, 10  $\mu$ m. **d**, Myosin levels are increased at the posterior boundary of Toll-2 stripes in *eve* mutants ( $P = 0.00001$ ). All edges oriented  $75^\circ$ – $90^\circ$  relative to the AP axis (AP) or edges only at anterior (Ant) or posterior (Post) boundaries of Toll-2 stripes; edge values were normalized to average edge intensity. **e**, Myosin levels are increased at the anterior boundary of ectopic Toll-2 and Toll-8 expression. **f**, Peak retraction velocities following laser ablation are increased at the anterior boundary of ectopic Toll-8 expression. Horizontal line, median; boxes, second and third quartiles; whiskers, 95% confidence interval. Single average values were obtained for each embryo; plots show the distribution of values across embryos.  $*P \leq 0.008$ ,  $**P \leq 0.0001$  (unpaired *t*-test). **d**, **e**,  $n = 6$ –15 embryos per genotype, **f**,  $n = 16$ –17 ablations per genotype (Supplementary Table 2).

normally do not aggregate, but cells expressing Toll-2, Toll-6, or Toll-8 aggregated with untransfected cells at high frequency, indicating that these receptors can bind to proteins present on S2R+ cells (Fig. 5e, f, k). Homophilic interactions between cells were not enhanced by Toll receptor expression (Fig. 5k). By contrast, Toll-2-positive cells formed extensive heterophilic contacts with cells expressing Toll-6 and/or Toll-8, creating chains of cells expressing alternating Toll receptors (Fig. 5g–k). Heterophilic interactions were not observed between cells expressing Toll-6 and Toll-8, which are often coexpressed within the same stripes (Fig. 1p). These results indicate that Toll-2 can promote heterophilic interactions with cells expressing Toll-6 or Toll-8. Embryos expressing any one receptor still display significant planar polarity and intercalary behaviour, suggesting that these proteins also interact with additional binding partners to generate planar polarity.

## Discussion

Together, these results demonstrate that the spatial signals that establish planar polarity and direct polarized cell behaviour during convergent extension in *Drosophila* are encoded at the cell surface by three Toll family receptors expressed in overlapping stripes along the AP axis of the embryo. Simultaneous disruption of Toll-2, Toll-6 and Toll-8 significantly impairs planar polarity, cell intercalation, and convergent extension, and removing one or two receptors disrupts planar polarity in distinct subsets of cells, indicating that these proteins serve non-redundant and highly localized functions. These findings support a model in which planar polarity is induced by interactions between neighbouring cells with different levels of Toll receptor activity (Fig. 5l). Therefore, *Drosophila* Toll receptors provide the basis of a spatial code that translates patterned *Eve* and *Runt* transcriptional activity into planar polarized actomyosin contractility, linking positional information provided by the embryonic AP patterning system to the essential cell behaviours that drive convergent extension. The Toll receptor code is incomplete in certain regions, such as the parasegmental boundaries, suggesting the existence of additional polarity cues at these interfaces. *Toll-2,6,8* mutants are similar to *runt* mutants with respect to all measures of cell

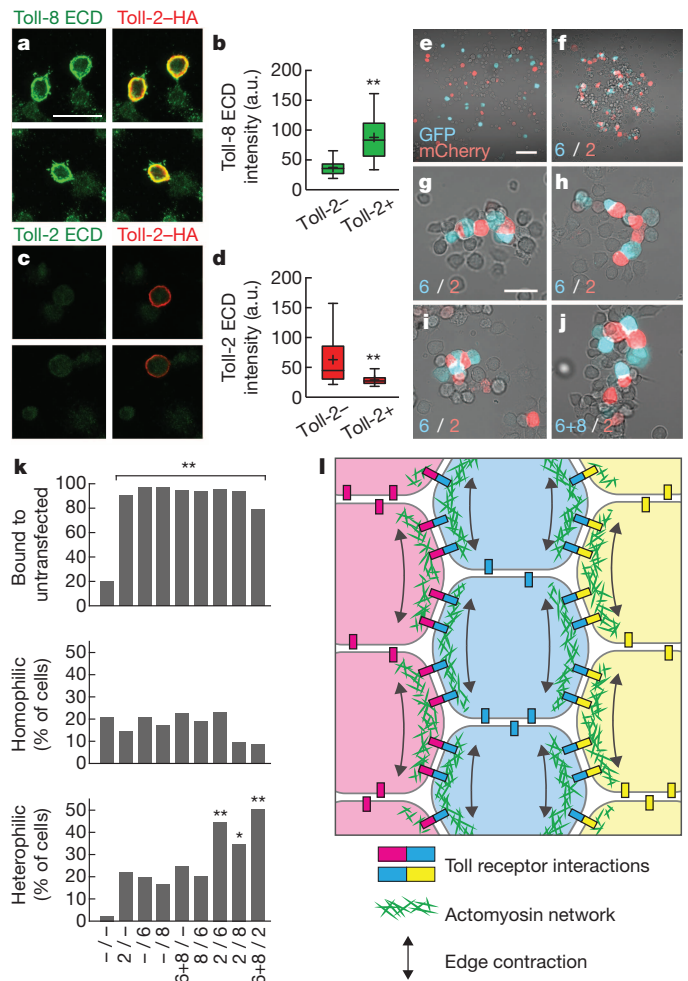


**Figure 5 | Toll receptors mediate heterophilic interactions between cells.** **a–d**, *Drosophila* S2R+ cells expressing Toll-2-HA (red) incubated with pentamerized Toll-8 ECD (green) or Toll-2 ECD (green). Toll-8 ECD bound more strongly (**b**) and Toll-2 ECD bound less strongly (**d**) to Toll-2-positive (Toll-2+) cells compared with Toll-2-negative (Toll-2-) cells ( $P < 0.00001$ , unpaired *t*-test). Horizontal line, median; boxes, second and third quartiles; whiskers, 95% confidence interval. **e–k**, Interactions between cells expressing myosin-GFP (cyan, sample listed before the / symbol) or myosin-mCherry (red, sample listed after the / symbol) with the indicated Toll receptors (–, myosin marker alone). Receptor-expressing cells displayed increased binding to untransfected cells ( $P \leq 0.0001$ , Chi-square test). Heterophilic binding was increased between cells expressing Toll-2 and Toll-6 ( $P \leq 0.0003$ ), Toll-2 and Toll-8 ( $P < 0.05$ ), and Toll-2 and Toll-6 + Toll-8 ( $P \leq 0.0001$ ) (Chi-square test).  $*P = 0.01$ – $0.05$ ,  $**P \leq 0.0003$ . **l**, Model showing heterophilic interactions between Toll receptors recruit myosin II, promoting oriented cell rearrangements and convergent extension. **b**, **d**,  $n = 170$ –176 cells per condition, **k**,  $n = 85$ –123 transfected cells per condition (Supplementary Table 2). Scale bars, 20  $\mu$ m (**a**, **c**, **g–j**), 100  $\mu$ m (**e**, **f**).

rearrangement and planar polarity, but are not as severe as *eve* mutants. Thus, although *Toll-2,6,8* mutants recapitulate much of the *eve* mutant phenotype, *Eve* likely has additional targets important for planar polarity.

Toll family receptors have a highly conserved structure in vertebrates and invertebrates, including extracellular LRR motifs that are often present in proteins involved in cell adhesion and cell–cell recognition<sup>43</sup>. Although individual receptors are not orthologous between flies and humans<sup>25</sup>, mammalian Toll-like receptors are required for epithelial regeneration and wound healing, processes that involve dynamic and spatially regulated changes in cell adhesion<sup>44–46</sup>. In the innate immune system, pathogen detection by Toll family receptors activates transcriptional pathways mediated by NF- $\kappa$ B and MAP kinase signalling<sup>23–26</sup>. However, the spatial information provided by patterned Toll receptor



expression in *Drosophila*, as well as the rapid timescale of cell rearrangements during convergent extension, suggest a more direct connection between Toll receptor signalling and the cellular contractile machinery. Consistent with this possibility, activation of mammalian Toll-like receptors in dendritic cells induces a rapid remodelling of the actin cytoskeleton<sup>47</sup> and mammalian Toll-like receptors can inhibit neurite outgrowth and trigger rapid growth cone collapse in neurons<sup>48,49</sup>, reminiscent of Toll receptor functions in the *Drosophila* nervous system<sup>40,41,50</sup>. Elucidating the mechanisms that link Toll family receptors to dynamic changes in cell polarity and behaviour may provide insight into conserved and relatively unexplored aspects of Toll receptor signalling.

**Online Content** Methods, along with any additional Extended Data display items and Source Data, are available in the online version of the paper; references unique to these sections appear only in the online paper.

**Received 9 May; accepted 9 October 2014.**

**Published online 2 November 2014.**

- Keller, R. *et al.* Mechanisms of convergence and extension by cell intercalation. *Phil. Trans. R. Soc. Lond. B* **355**, 897–922 (2000).
- Zallen, J. A. Planar polarity and tissue morphogenesis. *Cell* **129**, 1051–1063 (2007).
- Wallingford, J. B. Planar cell polarity and the developmental control of cell behavior in vertebrate embryos. *Annu. Rev. Cell Dev. Biol.* **28**, 627–653 (2012).
- Solnica-Krezel, L. & Sepich, D. S. Gastrulation: making and shaping germ layers. *Annu. Rev. Cell Dev. Biol.* **28**, 687–717 (2012).
- Walck-Shannon, E. & Hardin, J. Cell intercalation from top to bottom. *Nature Rev. Mol. Cell Biol.* **15**, 34–48 (2014).
- Zallen, J. A. & Wieschaus, E. Patterned gene expression directs bipolar planar polarity in *Drosophila*. *Dev. Cell* **6**, 343–355 (2004).
- Bertet, C., Sulak, L. & Lecuit, T. Myosin-dependent junction remodelling controls planar cell intercalation and axis elongation. *Nature* **429**, 667–671 (2004).
- Blankenship, J. T., Backovic, S. T., Sanny, J. S. P., Weitz, O. & Zallen, J. A. Multicellular rosette formation links planar cell polarity to tissue morphogenesis. *Dev. Cell* **11**, 459–470 (2006).
- Rauzi, M., Verant, P., Lecuit, T. & Lenne, P.-F. Nature and anisotropy of cortical forces orienting *Drosophila* tissue morphogenesis. *Nature Cell Biol.* **10**, 1401–1410 (2008).
- Fernández-González, R., Simões, S. de M., Röper, J.-C., Eaton, S. & Zallen, J. A. Myosin II dynamics are regulated by tension in intercalating cells. *Dev. Cell* **17**, 736–743 (2009).
- Nishimura, T. & Takeichi, M. Shroom3-mediated recruitment of Rho kinases to the apical cell junctions regulates epithelial and neuroepithelial planar remodeling. *Development* **135**, 1493–1502 (2008).
- Nishimura, T., Honda, H. & Takeichi, M. Planar cell polarity links axes of spatial dynamics in neural-tube closure. *Cell* **149**, 1084–1097 (2012).
- Lienkamp, S. S. *et al.* Vertebrate kidney tubules elongate using a planar cell polarity-dependent, rosette-based mechanism of convergent extension. *Nature Genet.* **44**, 1382–1387 (2012).
- Mahaffey, J. P., Grego-Bessa, J., Liem, K. F. & Anderson, K. V. Cofilin and Vangl2 cooperate in the initiation of planar cell polarity in the mouse embryo. *Development* **140**, 1262–1271 (2013).
- Shindo, A. & Wallingford, J. B. PCP and septins compartmentalize cortical actomyosin to direct collective cell movement. *Science* **343**, 649–652 (2014).
- Williams, M., Yen, W., Lu, X. & Sutherland, A. Distinct apical and basolateral mechanisms drive planar cell polarity-dependent convergent extension of the mouse neural plate. *Dev. Cell* **29**, 34–46 (2014).
- Irvine, K. D. & Wieschaus, E. Cell intercalation during *Drosophila* germband extension and its regulation by pair-rule segmentation genes. *Development* **120**, 827–841 (1994).
- Ninomiya, H., Elinson, R. P. & Winklbauer, R. Antero-posterior tissue polarity links mesoderm convergent extension to axial patterning. *Nature* **430**, 364–367 (2004).
- St Johnston, D. & Nüsslein-Volhard, C. The origin of pattern and polarity in the *Drosophila* embryo. *Cell* **68**, 201–219 (1992).
- Butler, L. C. *et al.* Cell shape changes indicate a role for extrinsic tensile forces in *Drosophila* germ-band extension. *Nature Cell Biol.* **11**, 859–864 (2009).
- Simões, S. de M. *et al.* Rho-kinase directs Bazooka/Par-3 planar polarity during *Drosophila* axis elongation. *Dev. Cell* **19**, 377–388 (2010).
- Wieschaus, E., Sweeton, D. & Costa, M. in *Gastrulation* 213–223 (Springer, 1992).
- Brennan, C. A. & Anderson, K. V. *Drosophila*: the genetics of innate immune recognition and response. *Annu. Rev. Immunol.* **22**, 457–483 (2004).
- Janeway, C. A. & Medzhitov, R. Innate immune recognition. *Annu. Rev. Immunol.* **20**, 197–216 (2002).
- Leulier, F. & Lemaitre, B. Toll-like receptors—taking an evolutionary approach. *Nature Rev. Genet.* **9**, 165–178 (2008).
- Kawai, T. & Akira, S. The role of pattern-recognition receptors in innate immunity: update on Toll-like receptors. *Nature Immunol.* **11**, 373–384 (2010).
- Tauszig, S., Jouanguy, E., Hoffmann, J. A. & Imler, J. L. Toll-related receptors and the control of antimicrobial peptide expression in *Drosophila*. *Proc. Natl Acad. Sci. USA* **97**, 10520–10525 (2000).
- Morisato, D. & Anderson, K. V. Signaling pathways that establish the dorsal-ventral pattern of the *Drosophila* embryo. *Annu. Rev. Genet.* **29**, 371–399 (1995).
- Chiang, C. & Beachy, P. A. Expression of a novel Toll-like gene spans the parasegment boundary and contributes to *hedgehog* function in the adult eye of *Drosophila*. *Mech. Dev.* **47**, 225–239 (1994).
- Kambris, Z., Hoffmann, J. A., Imler, J.-L. & Capovilla, M. Tissue and stage-specific expression of the *Tolls* in *Drosophila* embryos. *Gene Expr. Patterns* **2**, 311–317 (2002).
- Eldon, E. *et al.* The *Drosophila* 18 wheeler is required for morphogenesis and has striking similarities to Toll. *Development* **120**, 885–899 (1994).
- Keith, F. J. & Gay, N. J. The *Drosophila* membrane receptor Toll can function to promote cellular adhesion. *EMBO J.* **9**, 4299–4306 (1990).
- Kim, S., Chung, S., Yoon, J., Choi, K.-W. & Yim, J. Ectopic expression of Tollo/Toll-8 antagonizes Dpp signaling and induces cell sorting in the *Drosophila* wing. *Genesis* **44**, 541–549 (2006).
- Kleve, C. D., Siler, D. A., Syed, S. K. & Eldon, E. D. Expression of 18-wheeler in the follicle cell epithelium affects cell migration and egg morphology in *Drosophila*. *Dev. Dyn.* **235**, 1953–1961 (2006).
- Kolesnikov, T. & Beckendorf, S. K. 18 wheeler regulates apical constriction of salivary gland cells via the Rho-GTPase-signaling pathway. *Dev. Biol.* **307**, 53–61 (2007).
- Paré, A. *et al.* Visualization of individual *Scr* mRNAs during *Drosophila* embryogenesis yields evidence for transcriptional bursting. *Curr. Biol.* **19**, 2037–2042 (2009).
- Cermak, T. *et al.* Efficient design and assembly of custom TALEN and other TAL effector-based constructs for DNA targeting. *Nucleic Acids Res.* **39**, e82 (2011).
- Tamada, M., Farrell, D. L. & Zallen, J. A. Abi regulates planar polarized junctional dynamics through  $\beta$ -catenin tyrosine phosphorylation. *Dev. Cell* **22**, 309–319 (2012).
- Kasza, K. E., Farrell, D. L. & Zallen, J. A. Spatiotemporal control of epithelial remodeling by regulated myosin phosphorylation. *Proc. Natl Acad. Sci. USA* **111**, 11732–11737 (2014).
- McIlroy, G. *et al.* Toll-6 and Toll-7 function as neurotrophin receptors in the *Drosophila melanogaster* CNS. *Nature Neurosci.* **16**, 1248–1256 (2013).
- Ballard, S. L., Miller, D. L. & Ganetzky, B. Retrograde neurotrophin signaling through Tollo regulates synaptic growth in *Drosophila*. *J. Cell Biol.* **204**, 1157–1172 (2014).
- Özkan, E. *et al.* An extracellular interactome of immunoglobulin and LRR proteins reveals receptor–ligand networks. *Cell* **154**, 228–239 (2013).
- de Wit, J., Hong, W., Luo, L. & Ghosh, A. Role of leucine-rich repeat proteins in the development and function of neural circuits. *Annu. Rev. Cell Dev. Biol.* **27**, 697–729 (2011).
- Rakoff-Nahoum, S. & Medzhitov, R. Toll-like receptors and cancer. *Nature Rev. Cancer* **9**, 57–63 (2009).
- Grote, K., Schütt, H. & Schieffer, B. Toll-like receptors in angiogenesis. *Scientific World J.* **11**, 981–991 (2011).
- Huebener, P. & Schwabe, R. F. Regulation of wound healing and organ fibrosis by toll-like receptors. *Biochim. Biophys. Acta* **1832**, 1005–1017 (2013).
- West, M. A. *et al.* Enhanced dendritic cell antigen capture via toll-like receptor-induced actin remodeling. *Science* **305**, 1153–1157 (2004).
- Ma, Y. *et al.* Toll-like receptor 8 functions as a negative regulator of neurite outgrowth and inducer of neuronal apoptosis. *J. Cell Biol.* **175**, 209–215 (2006).
- Cameron, J. S. *et al.* Toll-like receptor 3 is a potent negative regulator of axonal growth in mammals. *J. Neurosci.* **27**, 13033–13041 (2007).
- Rose, D. *et al.* Toll, a muscle cell surface molecule, locally inhibits synaptic initiation of the RP3 motoneuron growth cone in *Drosophila*. *Development* **124**, 1561–1571 (1997).

**Supplementary Information** is available in the online version of the paper.

**Acknowledgements** We thank K. Anderson, K. Kasza, W. Razzell, G. Sabio, M. Shirasu-Hiza, A. Spencer, M. Tamada and R. Zallen for comments on the manuscript, B. Glick for the fast-folding YFP, M. Buszczak for pUASp-w-attB, and the BAC-Recombineering Core Facility at the University of Chicago for Toll-8-YFP. This work was funded by NIH/NIGMS grants GM079340 and GM102803 to J.A.Z. J.A.Z. is an Early Career Scientist of the Howard Hughes Medical Institute.

**Author Contributions** A.C.P., A.V. and J.A.Z. designed the study. A.C.P., A.V., C.T.F. and Z.M. performed the experiments, D.L.F. and A.M. performed the computational analysis, and A.C.P. and J.A.Z. wrote the manuscript. All authors participated in analysis of the data and in producing the final version of the manuscript.

**Author Information** The complete RNA sequencing data set is available on the Gene Expression Omnibus, accession code GSE61689. Reprints and permissions information is available at [www.nature.com/reprints](http://www.nature.com/reprints). The authors declare no competing financial interests. Readers are welcome to comment on the online version of the paper. Correspondence and requests for materials should be addressed to J.A.Z. ([zallenj@mskcc.org](mailto:zallenj@mskcc.org)).

## METHODS

**Drosophila stocks and genetics.** The following alleles were used: *Toll-2*<sup>Δ76</sup> (a deletion of 450 bp of the open reading frame and 2.3 kb of upstream sequence)<sup>34</sup>, *Toll-8*<sup>59</sup> (a deletion of the entire open reading frame)<sup>52</sup>, *Toll-8*<sup>145</sup> (a 1.2 kb deletion in the 5' UTR)<sup>35</sup>, *eve*<sup>R13</sup> (a frameshift that removes part of the homeodomain and the transcriptional repression domain)<sup>53</sup>, *runt*<sup>LB5</sup> (a deletion of the entire open reading frame)<sup>54</sup>, *Toll-6*<sup>1B</sup>, *Toll-6*<sup>5A</sup> and *Toll-7*<sup>14F</sup> (early frameshift mutations, this study). *Toll-8* mutant embryos were the progeny of *Resille-GFP*; *Toll-8*<sup>59/145</sup> flies. *Toll-2,6,8* triple mutants in Fig. 2 and Extended Data Fig. 3 were the progeny of *Toll-2*<sup>Δ76</sup>/*CyO*, *twi-Gal4*, *UAS-GFP*; *Toll-8*<sup>59</sup>, *Toll-6*<sup>5A</sup>, *Spider-GFP/eve-YFP* flies and were identified for live imaging by the absence of fluorescence from an *eve-YFP* transgene<sup>55</sup> (visible before imaging) and the absence of fluorescence from the *CyO*, *twi-Gal4*, *UAS-GFP* balancer (visible after imaging). *Toll-2,6,8* triple mutants in Fig. 3 and Extended Data Fig. 5 were the progeny of *Toll-2*<sup>Δ76</sup>/+; *Toll-8*<sup>59</sup>, *Toll-6*<sup>1B</sup>/*myosin-GFP* flies and were identified by the absence of *Toll-2* and *Toll-8* transcripts by *in situ* hybridization. The double-mutant chromosomes *Toll-7*, *Toll-2* and *Toll-8*, *Toll-6* were created using TALENs<sup>37</sup> to induce *Toll-7* and *Toll-6* null mutations on the *Toll-2*<sup>Δ76</sup> and *Toll-8*<sup>59</sup> chromosomes, respectively (Extended Data Fig. 4). Cell outlines were labelled with *Spider-GFP* (Fig. 2, Extended Data Fig. 3, and Supplementary Video 2), *Resille-GFP* (gift of A. Debec) (Fig. 2, Extended Data Fig. 3, and Supplementary Video 1), and *UAS-gap43-mCherry*<sup>56</sup> (Fig. 4f). Myosin II was visualized with a GFP fusion to the regulatory light chain expressed from the endogenous promoter<sup>57</sup>. In Fig. 4a–c, e, embryos were the progeny of *engrailed-Gal4* crossed to the following genotypes: (1) *UAS-β-catenin[AC]-HA* (II); *myosin-GFP* (III), (2) *myosin-GFP* (II); *UAS-Toll-2-HA* (III), (3) *UAS-Toll-8-HA* (II); *myosin-GFP* (III). In Fig. 4f, embryos were the progeny of *engrailed-Gal4* females crossed to *UAS-gap43-mCherry* males or *UAS-Toll-8-Venus*; *UAS-gap43-mCherry* males.

*Toll-8-YFP* was expressed from its endogenous regulatory sequences using BAC recombineering to introduce SYFP2, a fast-folding variant of YFP (gift of B. Glick), into BAC CH321-67E02, which spans 34 kb upstream and 27 kb downstream of the *Toll-8* open reading frame. To create *UAS-Toll-2-HA* and *UAS-Toll-8-HA*, the full-length *Toll-2* and *Toll-8* open reading frames were PCR amplified with primers containing a C-terminal HA tag and cloned into the pENTR/D-TOPO vector (Invitrogen). For *UAS-Toll-8-Venus*, full-length *Toll-8* was cloned into pENTR/D-TOPO, and Venus was subsequently cloned into the AscI site. *UAS* constructs were recombined into pUAS-w-attB (gift of Mike Buszczak) using Gateway cloning (Invitrogen). *UAS-Toll-8-HA*, *UAS-Toll-8-Venus* and the *Toll-8-YFP* BAC were targeted to the attP40 site on chromosome II and *UAS-Toll-2-HA* was targeted to the attP2 site on chromosome III by ΦC31-mediated transgenesis (Genetic Services).

**dsRNA generation.** Double-stranded RNAs (dsRNAs) designed to target *eve*, *runt*, *Toll-2*, *Toll-6*, *Toll-8* and *Toll-3* (negative control) were transcribed from PCR-generated templates containing T7 promoters on both ends. PCR templates (500 ng) were transcribed using the T7 MEGAscript kit (Life Technologies). The effects of *Toll-2/Toll-6* dsRNA injections into *Toll-8*<sup>59/145</sup> were confirmed with a second independent set of dsRNAs (#2 below) (Extended Data Fig. 3d). The dsRNAs were purified using gel-filtration spin columns (mini Quick Spin RNA Columns; Roche), precipitated with two volumes of isopropanol, washed with 75% ethanol, and resuspended in nuclease-free H<sub>2</sub>O. The dsRNA templates were amplified using the following primer pairs (all preceded by a T7 promoter sequence 5'-TAATACGACTCACTATAGGAGA-3'): *eve* (5'-TGCCATCCAGTCCGGATAACTCC-3' and 5'-CACACCCAGTCCGGTATAGCAGG-3'); *runt* (5'-ATGGTGGCAACAACACACAGGTC-3' and 5'-GCTTTGCTGTAGCTGGCGATCTGC-3'); *Toll-2* #1 (5'-AGTTTGAATCGAAACGCGAG-3' and 5'-GGACATGACCCGGATGT-3'); *Toll-2* #2 (5'-GCCTGCAACACAACAACATC-3' and 5'-TCAATGTGGCCAATGGAGT-3'); *Toll-6* #1 (5'-ATCGGCCAAAGAGCAGTA-3' and 5'-AGCAGCGTGTGCAGATTATT-3'); *Toll-6* #2 (5'-AATCAACCTTACGCGCATTGG-3' and 5'-AATCAACTTCAGCGCATTGG-3'); and *Toll-3* (5'-GAGCCTTGAACATTGGAGC-3' and 5'-CAGTTTCGCTGGAAGGTGAT-3').

**Embryo injections.** For RNA sequencing, pre-cellularized wild-type (Oregon-R) embryos (30–60 min after egg-laying) were dechorionated for 3 min in 50% bleach, immobilized with glue on coverslips, desiccated for ~7 min in an air-tight container with Drierite, covered with a 1:1 mixture of halocarbon oil 700 and 27 (Sigma), and micro-injected ventrally with *eve* and *runt* dsRNAs (1 μg μl<sup>-1</sup> each). Injected embryos were allowed to develop at 18 °C in a humid chamber until just before mesodermal invagination (late stage 5/early stage 6). Then, using a fine paintbrush, properly staged embryos were gently separated from the coverslip and transferred in a small drop of oil into 50 μl TRIzol reagent (Life Technologies). Approximately 60 staged embryos were collected per sample (3 biological replicates per condition) and frozen at –80 °C. Control embryos were injected with water but were otherwise treated identically.

For time-lapse imaging, pre-cellularized *Resille-GFP* embryos or the progeny of *Resille-GFP*; *Toll-8*<sup>59</sup>/*Toll-8*<sup>145</sup> flies were injected dorsally (30–60 min after egg laying) with dsRNA, as described above. Embryos injected with a single dsRNA were injected with 3 μg μl<sup>-1</sup> dsRNA, and embryos injected with two dsRNAs were injected with 1.5 μg μl<sup>-1</sup> of each dsRNA. The dsRNA-injected embryos were aged at 18 °C in a humid chamber until just before mesodermal invagination, detached from the coverslip using a fine paintbrush, and mounted for imaging in a thin layer of halocarbon oil between a coverslip and an oxygen-permeable membrane (YSI Life Sciences). Uninjected embryos were dechorionated immediately before imaging and mounted similarly.

**RNA sequencing.** We compared the transcriptomes of *eve* and *runt* dsRNA-injected (1 μg μl<sup>-1</sup> each) embryos with water-injected controls using RNA sequencing (50-bp paired end reads; 20 million reads per sample). Total RNA was extracted from ~60 staged embryos per sample, in triplicate, using a modified version of the TRIzol extraction protocol. Briefly, excess halocarbon oil was removed using a pipet, and the embryos were ground in microfuge tubes using RNase-free plastic pestles. An additional 450 μl TRIzol reagent was added, and the samples were incubated for 5 min at room temperature. Next, 100 μl chloroform was added, and the samples were incubated for 3 min at room temperature. Finally, the organic and aqueous phases were separated by centrifugation at 12,000g for 15 min. From this point onward, the manufacturer's protocol was followed. RNA sequencing was carried out by the MSKCC Genomics Core using the HiSeq platform (Illumina) with 50-bp paired-end reads and 20 million reads per sample. Fold-change analysis was carried out by the MSKCC Bioinformatics Core based on the number of reads per gene. *Toll-8* (*Tollo*) and *Toll-2* (*18w*) were strongly expressed and *Toll-6* and *Toll-7* were weakly expressed in the late stage 5/early stage 6 wild-type embryos used for analysis. *Toll* (*Tl*) is maternally and zygotically expressed at this stage<sup>51</sup>. Expression of the other *Drosophila* Toll family genes was not detected. The complete data set is available on the Gene Expression Omnibus (GSE61689).

**Quantitative RT-PCR.** Total RNA was isolated from dsRNA-injected embryos and uninjected controls, as described above. For each sample, 1 μg total RNA was DNase-treated and then reverse-transcribed using the High Capacity cDNA Reverse Transcription Kit (Applied Biosystems). Then 50 ng cDNA was amplified in each qRT-PCR reaction using pre-designed TaqMan gene expression assays for *Toll-2* (Dm01841837\_s1), *Toll-6* (Dm01822826\_s1), *Toll-7* (Dm01821614\_s1), *Toll-8* (Dm01837153\_s1) and *RpL32* (Dm02151827\_s1) (Applied Biosystems). Reactions were carried out using a 7900HT Fast Real-Time PCR system (Applied Biosystems). Relative expression levels were quantified using the 2<sup>-ΔΔC<sub>T</sub></sup> method<sup>58</sup>. The results are representative of three biological replicates and expression was normalized to *RpL32* within each sample.

**TALEN-mediated mutagenesis.** The TAL Effector Nucleotide Targeter 2.0 program (Cornell University) was used to design left and right TALEN targeting sequences immediately downstream of the transcriptional start sites of *Toll-6* and *Toll-7*. Targeting sequences contained upstream T nucleotides, were 15–20 bp in length, and the pairs were separated by 15–16-bp spacer regions. The targeting sequences were 5'-TGATCTACTATATGCTACTCA-3' (left) and 5'-GGCCAGGATCAGCAGCACA-3' (right) for *Toll-6*, and 5'-TGGCGGCAATCCTGCT-3' (left) and 5'-CTCCTGAGTCTCGCGGTGCA-3' (right) for *Toll-7*. The spacer regions for *Toll-6* (5'-TACTGCCCCGTGGTCT-3') and *Toll-7* (5'-GCTCCTGCTCGGGTT-3') contained *Ava*II and *Ava*I restriction sites, respectively, which were used to screen for deletions. The Golden Gate TALEN 2.0 kit<sup>37</sup> was used to construct the custom TALEN arrays (the NN RVD was used for G nucleotides). The final constructs were cloned into the RClscript-GoldyTALEN destination vector, and the mMessage mMachine T3 Kit (Invitrogen) was used to transcribe the TALEN RNAs. The Poly(A) Tailing Kit (Ambion) was used to add poly(A) tails to the RNA products, which were then purified using mini Quick Spin RNA columns (Roche).

Mixtures of left and right *Toll-7* or *Toll-6* TALEN mRNAs (250 ng μl each in H<sub>2</sub>O) were injected posteriorly into *Toll-2*<sup>Δ76</sup> and *Toll-8*<sup>59</sup> embryos, respectively. Injected males were individually crossed to balancer females, and the resulting F1 male progeny were again individually backcrossed to balancer females to establish stocks. DNA was extracted from the F1 males post-mating by crushing the flies in lysis buffer (10 mM Tris pH 8.2, 1 mM EDTA, 25 mM NaCl, and 200 μg ml<sup>-1</sup> proteinase K) and then incubating them for 30 min at 37 °C and 2 min at 95 °C. The following primers were used to amplify the genomic sequence surrounding the spacer regions: *Toll-6* (5'-CTTTGGCCAGCCAGTGAATTG-3' and 5'-AACAGATGGGCGAAAGATTGC-3') and *Toll-7* (5'-ATGTGCGCTTAGTGAAACAGTG-3' and 5'-GTCTGCAACCTGGCAAACTAGT-3'). The PCR products were digested overnight at 37 °C with *Ava*II or *Ava*I. Products showing restriction site loss were sequenced, and lines containing frame-shift mutations leading to premature translation termination were kept.

**Fluorescence *in situ* hybridization and immunohistochemistry.** Simultaneous fluorescence *in situ* hybridization and immunohistochemistry were carried out



using the acetone permeabilization method<sup>36,59</sup>. Hapten-tagged antisense RNA probes (~1,000 nt) were transcribed from PCR-generated templates containing a 3' T7 promoter, and probes were labelled by incorporating digoxigenin- or dinitrophenyl-tagged UTP nucleotides during transcription<sup>60</sup>. Primer sequences were: *Toll-2* (5'-TGCAACTGCTCAATCTCACC-3' and 5'-taatacgtactcataggagaTACTCCGACTCGATGCTGTG-3'); *Toll-6* (5'-ACCTTTGTGGGTCTGATTCG-3' and 5'-taatacgtactcataggagaTGCAGGATTCTTGCAGTTG-3'); *Toll-8* (5'-CTTCGGAGAGTTGGCTGAAC-3' and 5'-taatacgtactcataggagaTCTCATTCGTTGCTGTG-3'). Probes were fragmented by incubation in carbonate buffer (60 mM Na<sub>2</sub>CO<sub>3</sub> and 40 mM NaHCO<sub>3</sub>, pH 10.2) at 65 °C for 30 min. Hybridized probes were detected with mouse anti-digoxigenin (1:250; Jackson ImmunoResearch) or rabbit anti-dinitrophenyl (1:250; Molecular Probes) antibodies.

Toll-8-YFP embryos were fixed for 15 min in a 1:1 mixture of 18% formaldehyde (in 0.5× PBS) and heptane and manually devitellinized. Embryos in *engrailed-Gal4* misexpression experiments were fixed for 1 h in a 1:1 mixture of 3.7% formaldehyde (in 1× PBS) and heptane and manually devitellinized. Antibodies used were guinea pig anti-Runt (1:1,000)<sup>61</sup>, rabbit anti-GFP (1:150; Torrey Pines), guinea pig anti-Par-3 (1:100)<sup>8</sup>, and rat anti-HA (1:500; Roche). Primary antibodies were detected with Alexa Fluor-labelled secondary antibodies (1:500; Molecular Probes). Embryos were mounted in ProLong gold (Molecular Probes) and imaged on a Zeiss LSM700 laser-scanning confocal microscope with a PlanNeofluor 40×/1.3 NA oil-immersion objective; z-slices (1.0-μm thick) were acquired in steps of 0.5 μm.

**Time-lapse imaging.** Live imaging was performed on embryos expressing Spider-GFP, Resille-GFP or Myosin-GFP. Embryos were imaged using Perkin Elmer Ultra-View VOX or RS5 spinning-disk confocal microscopes with Plan-Neo 40×/1.3 NA or Plan-Apo 40×/1.3 NA oil-immersion objectives (Zeiss). Images were acquired using the Volocity software program. For Fig. 2, Extended Data Fig. 3, and Supplementary Videos 1 and 2, image stacks were acquired every 15 s at 1-μm z-steps and three apical planes in the region of the adherens junctions were projected for analysis. For Supplementary Videos 3–5, image stacks were acquired every 30 s at 0.5-μm z-steps and two apical planes were projected for analysis.

**Laser ablation.** Late stage 14/early stage 15 embryos were mounted in halocarbon oil and imaged using a Perkin Elmer RS5 spinning-disk confocal microscope with a Plan Neofluor 63×/1.4 NA oil-immersion objective (Zeiss), which was also used to focus the MicroPoint laser (Photonics Instruments). The velocity of edge retraction following ablation is predicted to be proportional to tension at the edge before ablation, assuming uniformity of tissue viscoelastic properties<sup>62</sup>. The laser was tuned to 365 nm and was used to ablate single cell interfaces at the anterior boundary of the *engrailed* expression domain, which was visualized by Gal4-dependent expression from UAS sequences present in the *sqh-Gap43-mCherry* transgene<sup>56</sup>. Image stacks were acquired every 3 s at 0.7-μm z-steps and peak retraction velocities were measured in ImageJ.

**Cell culture.** The coding regions for the Toll-2 and Toll-8 extracellular domains were cloned into the pENTR/D vector and then recombined into the pECIA14 expression vector (Addgene) using Gateway cloning. The pECIA14 vector contains an inducible CuSO<sub>4</sub> promoter and a C-terminal human placental alkaline phosphatase gene<sup>42</sup>. The constructs were transfected into *Drosophila* S2R+ cells (split one day earlier) using Cellfectin II reagent (Life Technologies), and protein expression was induced with 1 mM CuSO<sub>4</sub> 18 h post-transfection. The conditioned media was collected 3 days post-induction and concentrated for 15 min at 5,000g using Ultra-4 Centrifugal Filter Units (100 kDa cutoff; Amnicon). Next, 1× Complete, EDTA-free Protease Inhibitor Cocktail (Roche) and 0.02% sodium azide were added, and the media was stored at 4 °C until use.

S2R+ cells were maintained in Schneider's medium supplemented with 10% fetal calf serum at 25 °C. Cells were transfected with pActin5.1-GAL4 alone or in combination with UAS-Toll-2-HA or UAS-Toll-8-HA. One day post-transfection, cells were adhered to polylysine-coated coverslips for 10 min and washed with 1× PBS. Cells were then incubated 10 min with the concentrated media from cells expressing pentameric alkaline phosphatase fusions to the Toll-2 or Toll-8 extracellular domains diluted in Schneider's complete medium (protein levels were previously estimated by western blotting and normalized across samples). Cells were washed once with 1× PBS, fixed for 10 min with 4% formaldehyde/PBS, washed 3 times with 1× PBS, and blocked for 15 min in blocking buffer (1% BSA, 0.1% Triton, and 10 mM glycine). Cells were stained with rat anti-HA (1:250; Roche) and rabbit anti-human placental alkaline phosphatase (1:250; Serotec) primary antibodies and Alexa 488- and Alexa 647-conjugated secondary antibodies (1:500; Molecular Probes), mounted in Prolong Gold (Molecular Probes), and imaged using a Zeiss LSM700 confocal with a Plan-Apo 40×/1.3 NA oil-immersion objective. Cortical AP intensity was quantified using ImageJ.

For cell mixing experiments, S2R+ cells were transfected with appropriate combinations of pActin5.1-GAL4, *sqh*-myosin-GFP, UAS-myosin-mCherry, UAS-Toll-2, UAS-Toll-6-HA, and UAS-Toll-8-HA plasmids. Growing cells were added

to 6-well plates (2 ml Grace's medium/well) and transfected with 300 ng each plasmid diluted in 200 μl Grace's medium with 8 μl Cellfectin II reagent (Invitrogen). The next day, transfected cells were counted using a haemocytometer, and 10<sup>6</sup> cells from each condition (2 × 10<sup>6</sup> cells total) were combined in a final volume of 2 ml in 50 ml Falcon tubes. The tubes were placed vertically on a tabletop shaker and gently agitated for 3 h at 100 r.p.m. A portion of each mixture (600 μl) was pipetted using a blunt-cut P1000 tip and allowed to adhere to polylysine-coated coverslips for 45 min. The semi-adherent cells were then washed once with 1× PBS, fixed for 10 min with 4% formaldehyde/PBS, washed 3 times with 1× PBS, and then mounted in Prolong Gold. Similar results were observed with the fluorescent markers reversed. We did not observe binding between cells expressing Toll-6 or Toll-8 and the extracellular domains of Toll-2 or Toll-8 in this assay (data not shown).

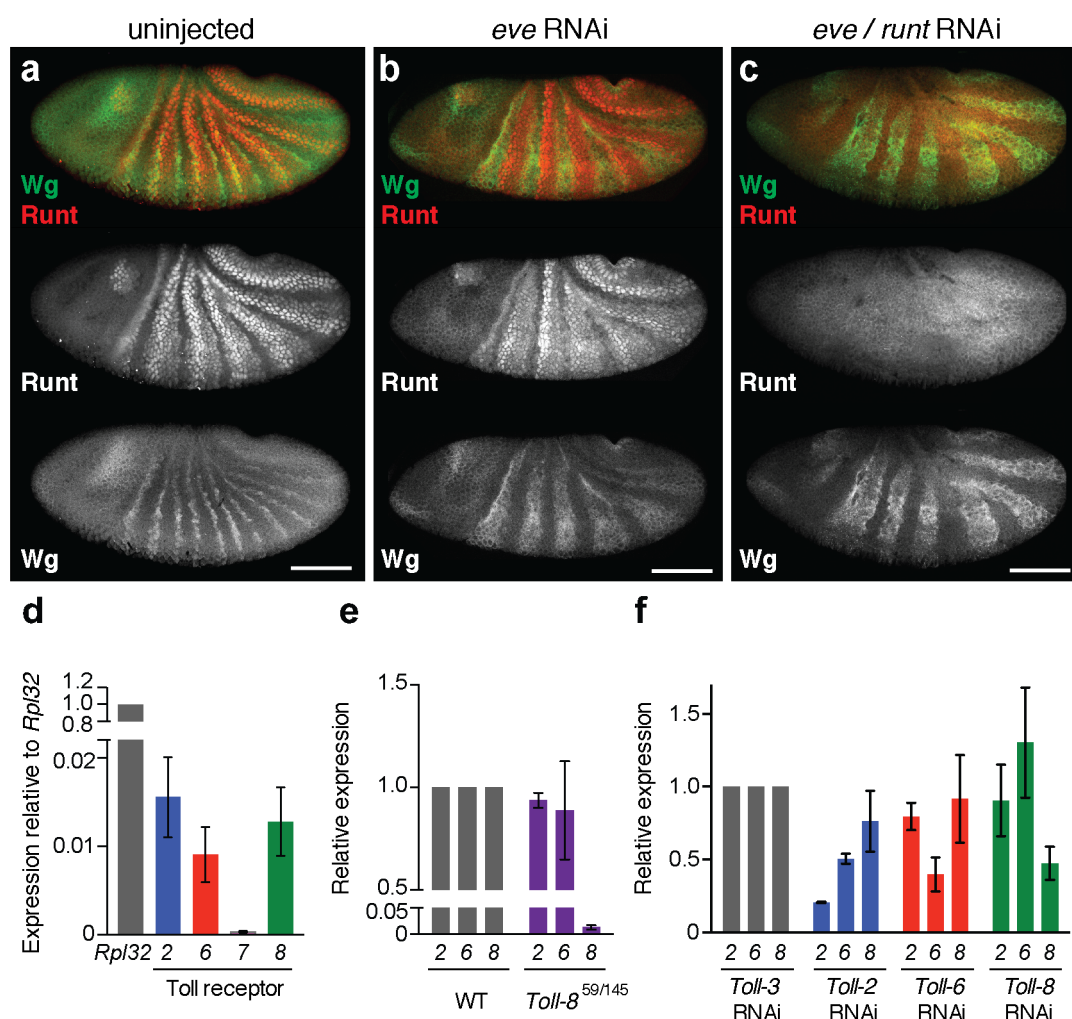
**Image analysis.** Time-lapse movies were segmented and analysed using custom software implemented in MATLAB. The onset of elongation was  $t = 0$ , set as the point at which the derivative of tissue AP length plotted over time intersects zero. Tissue length was measured as the long axis of an ellipse fit to the group of tracked cells. Cell rearrangements (neighbours lost per cell) were calculated as the number of cell boundaries that contracted to a vertex and did not reform over the course of the movie, divided by the total number of tracked cells. Cells tracked  $\geq 12.5$  min after  $t = 0$  were analysed for cell rearrangement and cells tracked from  $t = 0$  until the end of the movie were analysed for axis elongation. Edge contraction rate was analysed at mid-stage 7 (in the period spanning 5–8 min after the onset of elongation, inclusive) and was the average rate of change in length over a sliding 15-frame time window (15 s between frames) for all edges that ultimately contracted to a vertex and were oriented 75–90° relative to the AP axis. The first-order derivatives of the time series for individual edges were identified using a Savitzky-Golay filter implemented in MATLAB. Edge formation errors were followed by visual inspection. Statistical analysis was performed using the *F*-test followed by the appropriate *t*-test for equal variance (Student's *t*-test) or unequal variance (Welch's *t*-test), using the value at  $t = 30$  min as the test statistic. *P* values were determined by comparison to the most appropriate control: wild-type *Spider-GFP* for comparison to mutant embryos expressing *Spider-GFP*, wild-type *Resille-GFP* for comparison to mutant embryos expressing *Resille-GFP*, and control-injected *Resille-GFP* (injected with *Toll-3* dsRNA) for comparison to dsRNA-injected embryos expressing *Resille-GFP*.

Planar polarity was analysed at single-cell resolution in fixed embryos using maximum intensity projections of the apical junctional domain. Cell boundaries were identified using custom segmentation software implemented in MATLAB. Myosin II and Par-3 intensity was the average pixel intensity along each edge, with the intensity of each pixel calculated as the maximum pixel intensity on a 5-pixel-wide line oriented perpendicular to the edge. Following background subtraction based on the cytoplasmic intensities of the 20 closest cells, the ratio of the average intensity of AP edges (edges oriented 60–90° to the AP axis) to the average intensity of DV edge (0–30°) was calculated for each cell, and a single average value was obtained for each embryo (full distributions shown in Extended Data Fig. 5). Cells without at least one AP and one DV edge were not scored (grey cells in Extended Data Fig. 6a). For Fig. 4d, the average fluorescence intensity at the indicated classes of AP edges was normalized to the average intensity of all edges within the same embryo. For Fig. 4e, the average myosin-GFP intensity at the anterior boundary of the *engrailed* domain was normalized to the average myosin-GFP intensity in the adjacent smooth cells. Increased myosin recruitment was not observed at the posterior boundary of the *engrailed* domain, although the formation of actin-based denticle structures in these cells may preclude induction of ectopic actomyosin polarity.

- Gerttula, S., Jin, Y. & Anderson, K. V. Zygotic expression and activity of the *Drosophila* Toll gene, a gene required maternally for embryonic dorsal-ventral pattern formation. *Genetics* **119**, 123–133 (1988).
- Yagi, Y., Nishida, Y. & Ip, Y. T. Functional analysis of Toll-related genes in *Drosophila*. *Dev. Growth Differ.* **52**, 771–783 (2010).
- Nüsslein-Volhard, C. & Wieschaus, E. Mutations affecting segment number and polarity in *Drosophila*. *Nature* **287**, 795–801 (1980).
- Duffy, J. B. & Gergen, J. P. The *Drosophila* segmentation gene *runt* acts as a position-specific numerator element necessary for the uniform expression of the sex-determining gene *Sex-lethal*. *Genes Dev.* **5**, 2176–2187 (1991).
- Ludwig, M. Z., Manu, K., Kitter, R., White, K. P. & Kreitman, M. Consequences of eukaryotic enhancer architecture for gene expression dynamics, development, and fitness. *PLoS Genet.* **7**, e1002364 (2011).
- Martin, A. C., Gelbart, M., Fernández-González, R., Kaschube, M. & Wieschaus, E. F. Integration of contractile forces during tissue invagination. *J. Cell Biol.* **188**, 735–749 (2010).
- Royou, A., Field, C., Sisson, J. C., Sullivan, W. & Kares, R. Reassessing the role and dynamics of nonmuscle myosin II during furrow formation in early *Drosophila* embryos. *Mol. Biol. Cell* **15**, 838–850 (2004).
- Schmittgen, T. D. & Livak, K. J. Analyzing real-time PCR data by the comparative C<sub>T</sub> method. *Nature Protocols* **3**, 1101–1108 (2008).

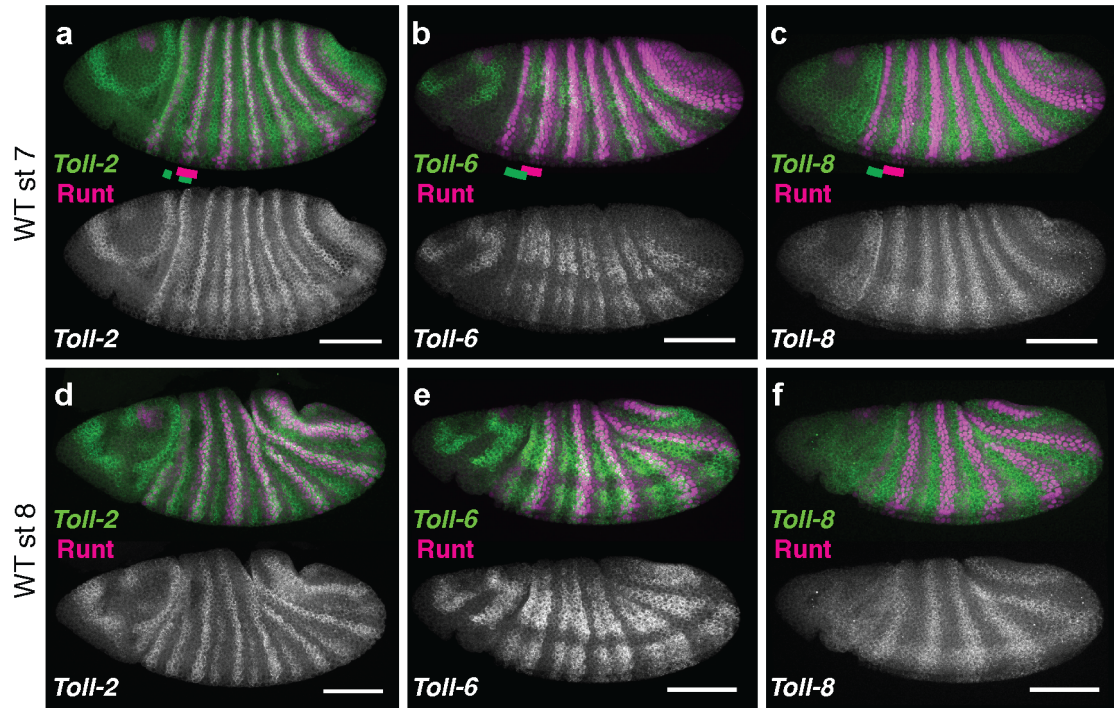
59. Nagaso, H., Murata, T., Day, N. & Yokoyama, K. K. Simultaneous detection of RNA and protein by *in situ* hybridization and immunological staining. *J. Histochem. Cytochem.* **49**, 1177–1182 (2001).
60. Kosman, D. *et al.* Multiplex detection of RNA expression in *Drosophila* embryos. *Science* **305**, 846 (2004).
61. Kosman, D., Small, S. & Reinitz, J. Rapid preparation of a panel of polyclonal antibodies to *Drosophila* segmentation proteins. *Dev. Genes Evol.* **208**, 290–294 (1998).
62. Hutson, M. S. *et al.* Forces for morphogenesis investigated with laser microsurgery and quantitative modeling. *Science* **300**, 145–149 (2003).





**Extended Data Figure 1 | Targeting of Eve, Runt and Toll receptors by dsRNA injection.** **a–c**, Control and dsRNA-injected embryos stained for Runt (red, middle) and Wingless (Wg) (green, bottom) proteins. **a**, In uninjected wild-type embryos, Runt is expressed in seven broad stripes and Wg is expressed in 14 narrow stripes. **b**, In embryos injected with *eve* dsRNA alone, Runt is more uniformly expressed, and the Wg expression pattern collapses into fewer, broader stripes, similar to *eve* mutants (data not shown). **c**, In embryos co-injected with *eve* and *runt* dsRNAs, Runt protein is undetectable, indicating that the *runt* dsRNA effectively inhibits Runt expression, and the Wg expression pattern collapses into fewer, broader stripes, similar to *eve* and *runt* mutants (data not shown). Anterior left, ventral down. Scale bars, 100  $\mu$ m.

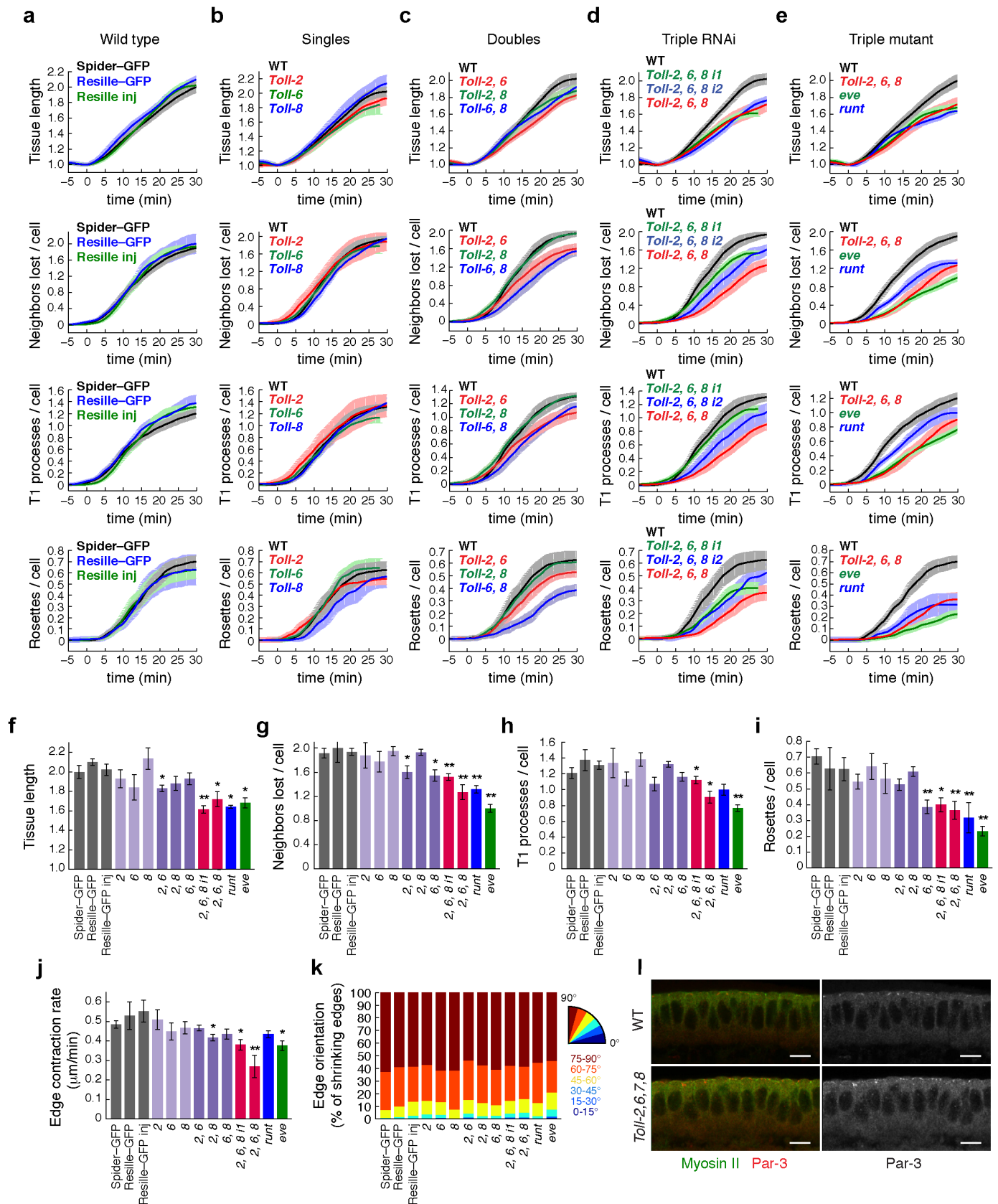
**d–f**, Quantitative RT–PCR analysis of *Toll-2* (2), *Toll-6* (6), *Toll-7* (7) and *Toll-8* (8) expression in late stage 6 embryos before axis elongation.  $C_T$  values were normalized to the internal control gene *Rpl32*. **d**, Relative transcript levels in WT embryos were calculated using the  $2^{-\Delta C_T}$  method. *Toll-2*, *Toll-6* and *Toll-8* were expressed at comparable levels, whereas *Toll-7* was expressed at much lower levels. **e**, *Toll-8* expression in *Toll-8*<sup>59/145</sup> embryos was reduced 76-fold compared with WT embryos. **f**, Gene expression was specifically reduced in embryos injected with single dsRNAs targeting *Toll-2*, *Toll-6* or *Toll-8* compared with embryos injected with a control *Toll-3* dsRNA, as determined using the  $2^{-\Delta C_T}$  method.



**Extended Data Figure 2 | Expression patterns of *Toll-2*, *Toll-6* and *Toll-8* relative to *Runt*.** a–f, *Toll-2*, *Toll-6* and *Toll-8* transcripts (green top, white bottom) and *Runt* protein (magenta) in wild-type (WT) embryos during early (stage 7, a–c) and mid-elongation (stage 8, d–f). The embryos are the same as in

Fig. 1a–f. Coloured bars indicate the position of the *Toll-2*, *Toll-6* and *Toll-8* stripes (green) relative to *Runt* (magenta). Anterior left, ventral down. Scale bars, 100  $\mu$ m.

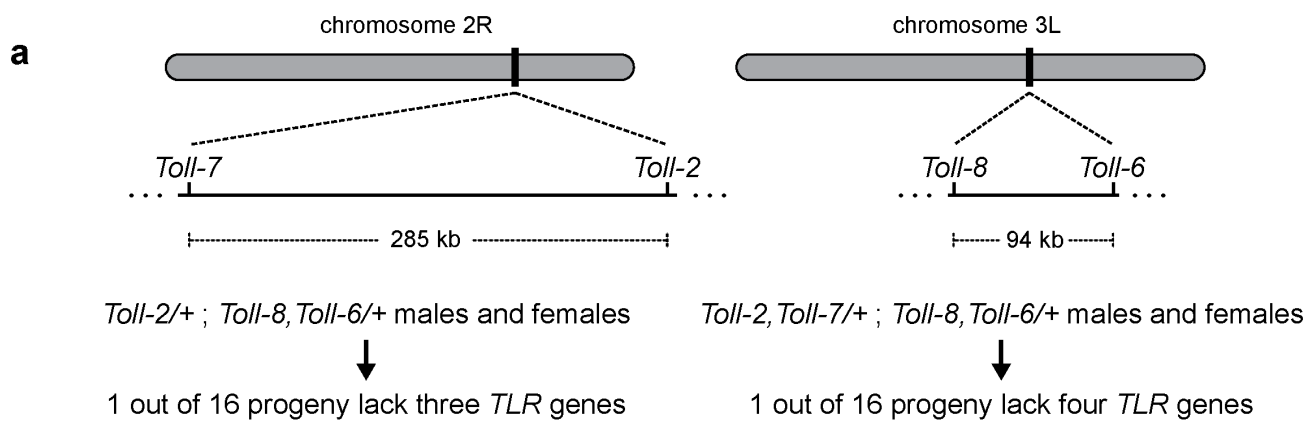




**Extended Data Figure 3 | Time-lapse imaging of embryos defective for combinations of *Toll-2*, *Toll-6* and *Toll-8*.** **a–e**, Axis elongation (tissue AP length relative to  $t = 0$ ) (first row), total cell rearrangements (average number of neighbours lost per cell) (second row), T1 processes resulting from the contraction of single edges<sup>7</sup> (third row), and rosette rearrangements resulting from the contraction of multiple connected edges<sup>8</sup> (fourth row) over time in wild-type embryos (**a**) and embryos defective for one (**b**), two (**c**), or three (**d**, **e**) Toll receptors. Images were acquired every 15 s. **f–i**, Axis elongation (**f**), average number of cell rearrangements (**g**), T1 processes (**h**), and rosettes (**i**) per cell at  $t = 30$  min. **j**, Edge contraction rate for AP edges (oriented  $75\text{--}90^\circ$  relative to the AP axis) at mid-stage 7 (averaged from  $t = 5\text{--}8$  min after the onset of elongation). **k**, The orientation of shrinking edges relative to the AP axis ( $0^\circ$ ) was similar for all conditions. Single average values were obtained for each embryo, and plots show the mean  $\pm$  s.e.m. across embryos. \* $P = 0.01\text{--}0.03$ , \*\* $P < 0.005$  (unpaired  $t$ -test).  $n = 3\text{--}8$  embryos per genotype, 164–365

cells per embryo (see Supplementary Table 2 for full list of  $n$  values). **l**, Cross sections of the ventrolateral epithelium in wild-type and *Toll-2* <sup>$\Delta 76$</sup> , *Toll-6* <sup>$1B$</sup> , *Toll-7* <sup>$14F$</sup> , *Toll-8* <sup>$59$</sup>  mutant (*Toll-2,6,7,8*) embryos, showing that apical–basal polarity is unaffected in quadruple mutants. Myosin II (green) and Par-3 (red, white) are enriched at apical adherens junctions. Apical up, basal down. Scale bars, 10  $\mu$ m. WT (*Spider-GFP* in **a**, **e–k**; *Resille-GFP* in **a**, **f–k**; and *Resille-GFP* + *Toll-3* dsRNA in **a–d** and **f–k**); *Toll-2* (*Resille-GFP* + *Toll-2* dsRNA); *Toll-6* (*Resille-GFP* + *Toll-6* dsRNA); *Toll-8* (*Resille-GFP*; *Toll-8* <sup>$59/145$</sup> ); *Toll-2,6* (*Resille-GFP* + *Toll-2/Toll-6* dsRNAs); *Toll-2,8* (*Resille-GFP*; *Toll-8* <sup>$59/145$</sup>  + *Toll-2* dsRNA); *Toll-6,8* (*Toll-2* <sup>$\Delta 76$</sup> /CyO; *Toll-8* <sup>$59$</sup> , *Toll-6* <sup>$5A$</sup> , *Spider-GFP*); *Toll-2,6,8* (*Toll-2* <sup>$\Delta 76$</sup> ; *Toll-8* <sup>$59$</sup> , *Toll-6* <sup>$5A$</sup> , *Spider-GFP*), *Toll-2,6,8 i1* (*Resille-GFP*; *Toll-8* <sup>$59/145$</sup>  + *Toll-2/Toll-6* dsRNAs set 1); *Toll-2,6,8 i2* (*Resille-GFP*; *Toll-8* <sup>$59/145$</sup>  + *Toll-2/Toll-6* dsRNAs set 2); *runt* (*runt* <sup>$1B5$</sup> ; *Spider-GFP/+*); and *eve* (*eve* <sup>$R13$</sup> ; *Spider-GFP/+*).





**b** TALEN-induced *Toll-6* frameshift mutations on *Toll-8*<sup>59</sup> chromosome III

*Toll-6* ATGATCTACTATATGCTACTCA**TACTGCCCCGTTGGTCTCT**GGCCCAGGATCAGCAGCACACCACGGAATCGTGTGC...

*Toll-6 [1B]* ATGATCTACTATATGCTACTCA-----GATCAGCAGCACactACGGAATCGTGTGC... (23 bp deletion)

*Toll-6 [4B]* ATGATCTACTATATGCTACTCATACTG-----TCCTGGCCCAGGATCAGCAGCACactACGGAATCGTGTGC... (7 bp deletion)

*Toll-6 [5A]* ATGATCTACTATATGCTACTCATACTGCC-----AGGATCAGCAGCACACCACGGAATCGTGTGC... (13 bp deletion)

### Predicted amino-acid sequences of mutant Toll-6 proteins

Toll-6 **MIYYMLLILPVVLAQDQQHTTESLSTKHHQQQQLSHSNAIMGEAGVSNSQLMQPSTPARTLRPLTAQQQQLSHS...** (1513 aa)  
Toll-6 [18] **MIYYMLLRSAAHYGIAVHQAPPAATAVALECDNG\*** (34 aa)  
Toll-6 [48] **MIYYMLLILSWPRISSTLNRNCPSTSSSSCRTRMR\*** (35 aa)  
Toll-6 [5A] **MIYYMLLILPRISSTLNRNCPSTSSSSCRTRMR\*** (37 aa)

**c** TALEN-induced *Toll-7* frameshift mutations on *Toll-2*<sup>Δ76</sup> chromosome II

## Deletions

*Toll-7* ATGGCGCAATCCTGCTGCTCTCTCTGAGTCTCGCGTCTGAGTCCGCACTGGCGCCCAAGGA...  
*Toll-7 [1C]* ATGGCGCAATCCTGCTGCTCC-----GGTTCTCTGAGTCTCGCGTCTGAGTCCGCACTGGCGCCCAAGGA... (5 bp deletion)  
*Toll-7 [5F]* ATGGCGCAATCCTGCTGCTCC-----GGTTCTCTGAGTCTCGCGTCTGAGTCCGCACTGGCGCCCAAGGA... (5 bp deletion)  
*Toll-7 [4D]* ATGGCGCAATCCTG-----GAGTCTCGCGTCTGAGTCCGCACTGGCGCCCAAGGA... (23 bp deletion)  
*Toll-7 [16A]* ATGGCGCAATCCTG-----GGTTCTCTGAGTCTCGCGTCTGAGTCCGCACTGGCGCCCAAGGA... (13 bp deletion)

## Insertions

Toll-7 ATGGCGCAATCTCTGCT**GCTCCTGC**----**TCGGGTTCT**CTCTGGAGTCTCGCGGT**CGA**GTCGCACTGGCGCCCA...

Toll-7 [5A] ATGGCGCAATCTCTGCTGCTCCTCGagcaqGGGTTCT**CTCTGGAGTCTCGCGGT**CGAGTCCGCACTGGCGCCCA... (T>AGCAG)

## Nucleotide changes

Toll-7 **A**TGGCGGCAATCTGCT**G**CTCTCTGCTCGGGTTCTCTGGAGTCTCGCGGTCGAGTCCGCACCTGGCGCCCAAGGA...

Toll-7 [14F] ATGGCGGCAATCTGCTGCAatcca--GGGTTCTCTGGAGTCTCGCGGTCGAGTCCGCACCTGGCGCCCAAGGA... (TCCTGCTC>AATCCA)

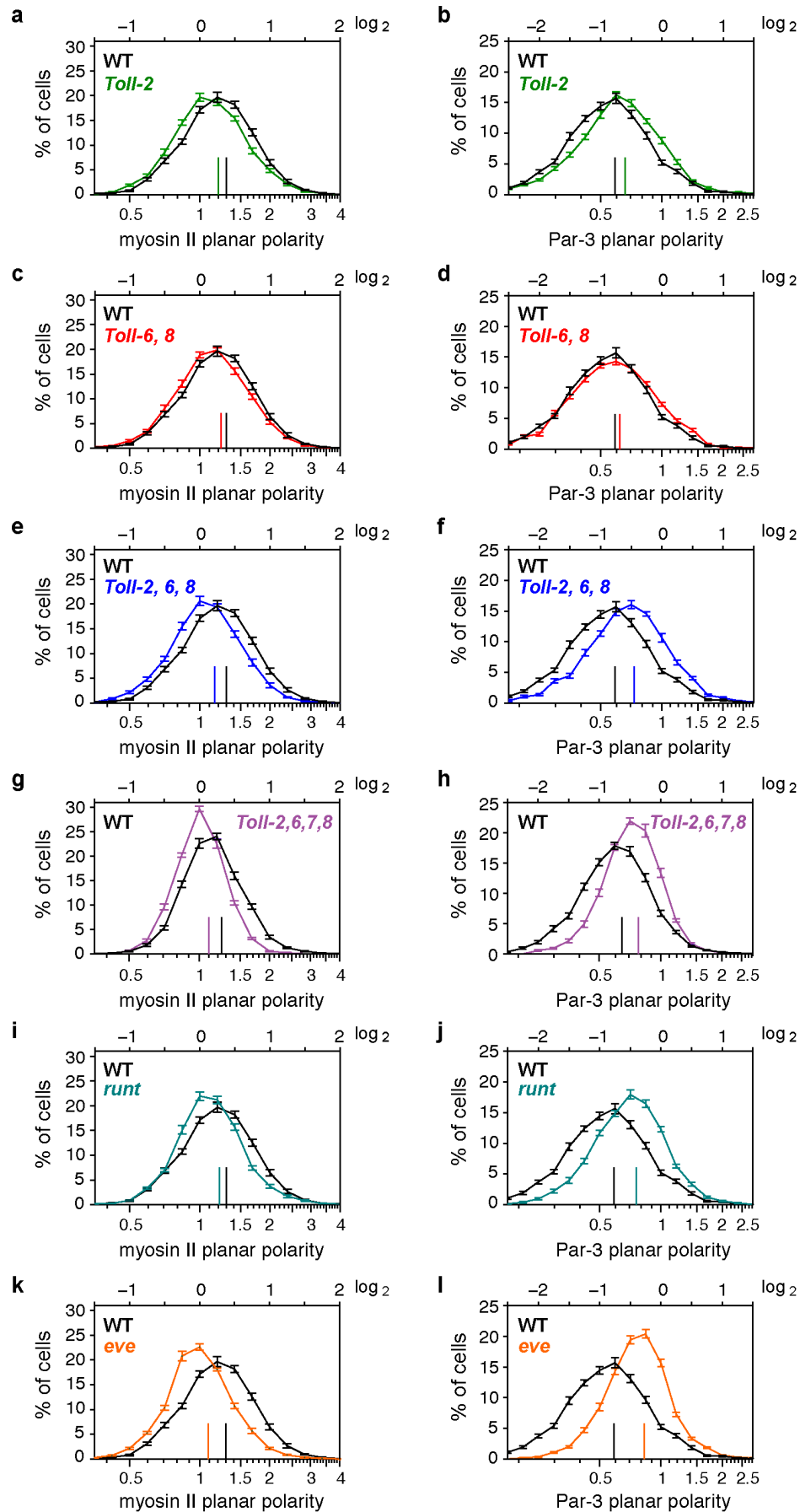
### Predicted amino-acid sequences of mutant Toll-7 proteins

Toll-7  
Toll-7 [1C]  
Toll-7 [4D]  
Toll-7 [5A]  
Toll-7 [5F]  
Toll-7 [14F]  
Toll-7 [16A]

MAAII L L L L L L G F S W S L A V E S A L A P K E S E S S A M L G A G T G A A A T V S L S G D Y S S L L S N V P A A S P V P A N P S Q P S G P A N Q C S W S Y N G T S S V H C A L R I ... (1446 aa)  
MAAII L L L R V L L E S R G R V R T G A Q G E R I E C Q R H V R R R N R S R C H S I A I R L L L L A A V C A G R L A G S G Q S I A T Q W P G Q P V L L V L Q R H Q F G A L R P A S H \* (92 aa)  
MAAII L L E S R G R V R T G A Q G E R I E C Q R H V R R R N R S R C H S I A I R L L L L A A V C A G R L A G S G Q S I A T Q W P G Q P V L L V L Q R H Q F G A L R P A S H \* (86 aa)  
MAAII L L L Q R V L L E S R G R V R T G A Q G E R I E C Q R H V R R R N R S R C H S I A I R L L L L A A V C A G R L A G S G Q S I A T Q W P G Q P V L L V L Q R H Q F G A L R P A S H \* (95 aa)  
MAAII L L L R V L L E S R G R V R T G A Q G E R I E C Q R H V R R R N R S R C H S I A I R L L L L A A V C A G R L A G S G Q S I A T Q W P G Q P V L L V L Q R H Q F G A L R P A S H \* (92 aa)  
MAAII L Q S R V L L E S R G R V R T G A Q G E R I E C Q R H V R R R N R S R C H S I A I R L L L L A A V C A G R L A G S G Q S I A T Q W P G Q P V L L V L Q R H Q F G A L R P A S H \* (93 aa)  
MAAII L G S P G V S R S S P H W R P R R A N P A P C \* (29 aa)

**Extended Data Figure 4 | Generation of double, triple and quadruple Toll receptor mutants.** **a**, The crossing strategy used to generate *Toll*-2,6,8 triple mutants and *Toll*-2,6,7,8 quadruple mutants. *Toll*-7 and *Toll*-2 are 285 kb apart on the right arm of chromosome II and *Toll*-8 and *Toll*-6 are 94 kb apart on the left arm of chromosome III. **b**, Three unique *Toll*-6 null alleles (*Toll*-6<sup>1B</sup>, *Toll*-6<sup>4B</sup> and *Toll*-6<sup>5A</sup>) were generated on the *Toll*-8<sup>59</sup> chromosome using TALEN-mediated mutagenesis to create *Toll*-8, *Toll*-6 double-mutant chromosomes. **c**, Six unique *Toll*-7 null alleles (*Toll*-7<sup>1C</sup>, *Toll*-7<sup>4D</sup>, *Toll*-7<sup>5A</sup>, *Toll*-7<sup>5F</sup>, *Toll*-7<sup>14F</sup> and *Toll*-7<sup>16A</sup>) were generated on the *Toll*-2<sup>A76</sup> chromosome using TALEN-mediated mutagenesis to create *Toll*-7, *Toll*-2 double-mutant

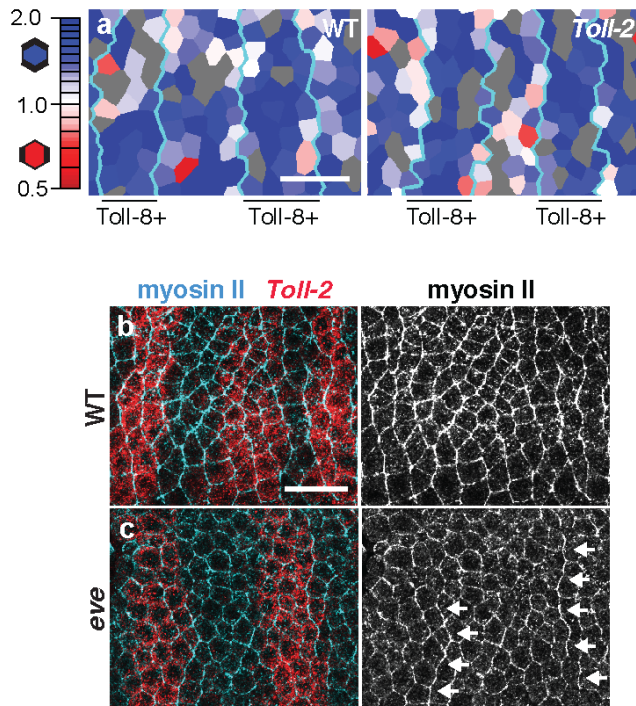
chromosomes. Each *Toll-6* and *Toll-7* allele is a frame-shift mutation leading to premature translational termination. TALENs were designed to induce double-stranded breaks immediately downstream of the ATG translational start sites. Orange letters indicate the TALEN binding sites, and the spacer regions are shown in bold. The *Ava*II and *Ava*I restriction sites used for screening are indicated with dotted boxes. Shown below are the predicted amino acid sequences of the mutant proteins compared with the wild-type sequence. Residues that are identical in the mutant and wild-type proteins are shown in green.



**Extended Data Figure 5 | Distributions of cell polarity measurements in Toll receptor mutants.** **a–l**, Planar polarity distributions for myosin II (left panels) and Par-3 (right panels) in *Toll-2* single mutants (**a, b**), *Toll-6,8* double mutants (**c, d**), *Toll-2,6,8* triple mutants (**e, f**), *Toll-2,6,7,8* quadruple mutants (**g, h**), *runt* mutants (**i, j**) and *eve* mutants (**k, l**). Vertical lines indicate the means of the distributions. Error bars indicate s.e.m. between embryos. Mean planar polarity was shifted towards 1 (absolute ratio; 0 on the  $\log_2$  scale) in *Toll-2* single mutants ( $P = 0.005$  for myosin and  $P < 0.00005$  for Par-3), *Toll-2,6,8* triple mutants ( $P < 0.00002$  for myosin and Par-3), *Toll-2,6,7,8* quadruple

mutants ( $P < 0.00001$  for myosin and Par-3), *runt* mutants ( $P = 0.002$  for myosin and  $P < 0.00001$  for Par-3) and *eve* mutants ( $P < 0.00001$  for myosin and Par-3), indicating reduced planar polarity (unpaired *t*-test with the means of the distributions used as the test statistic). Planar polarity in *Toll-2,6,7,8* quadruple mutants was not significantly enhanced relative to triple mutants. Single values were obtained for each embryo, and plots show the mean  $\pm$  s.e.m. across embryos.  $n = 2,166$ – $4,909$  cells in 7–20 embryos per genotype (Supplementary Table 2).





**Extended Data Figure 6 | Toll receptor expression affects planar polarity in a regional manner.** **a**, Single-cell analysis of Par-3 planar polarity in wild-type (WT) (left) and *Toll-2* mutant (right) embryos. *Toll-8*-expressing cells were identified by fluorescence *in situ* hybridization. Cyan lines, boundaries between stripes; *Toll-8*+, *Toll-8*-expressing cells. AP enriched (red), DV enriched (blue). Cells without at least one AP and one DV edge were not scored (grey). **b**, **c**, Myosin II (cyan, white) and *Toll-2* mRNA (red) in stage 7 WT (**b**) and *eve* mutant (**c**) embryos. Arrows, residual myosin cables in *eve* embryos. Anterior left, ventral down. Scale bars, 20  $\mu$ m.